Advanced Physical Research
Vol.7, No.3, 2025, pp.203-214
https://doi.org/10.62476/apr.73203

DARK PHOTON PHENOMENOLOGY AT ELECTRON-POSITRON COLLIDERS: ANALYTICAL PREDICTIONS AND EXPERIMENTAL PROBES

Amina Berkane*

Laboratory of Physics and Chemistry of Materials, Department of Physics,
University of M'Sila, Algeria

Abstract. The dark photon, a hypothetical gauge boson arising from an additional hidden gauge symmetry, represents a compelling extension of the Standard Model and a potential portal to the dark matter sector. In scenarios where its mass lies significantly below the electroweak scale, the dark photon may kinetically mix with the Standard Model photon through a small parameter ε, leading to feeble interactions with charged particles. This work investigates the production and detection prospects of such a dark photon in high-luminosity collider environments. Using Feynman diagrammatic techniques, we present complete analytical derivations of the kinetic mixing Lagrangian, decay widths, and cross-sections for processes such as $e^+e^- \to \gamma U$. We provide step-by-step calculations of the differential and total cross-sections, analyze their dependence on the dark photon mass m_U and kinetic mixing ε, and compare the results with exclusion limits from Belle II and KLOE-2. The novelty of our work lies in the explicit analytical treatment, updated numerical simulations incorporating ISR effects, and new exclusion plots that extend previous analyses. The findings offer guidance for current and future searches at electron-positron colliders.

Keywords: Dark photon, hidden gauge sector, kinetic mixing, electron-positron collisions, Feynman diagrams, cross-section computation.

Corresponding author: Amina Berkane, Laboratory of Physics and Chemistry of Materials, Department of Physics, University of M'Sila, Algeria, e-mail: *Amina.berkane@univ-msila.dz*

Received: 6 August 2025; Revised: 26 August 2025; Accepted: 28 August 2025; Published: 16 October 2025.

1 Introduction

Observations in cosmology and astrophysics show that about 85% of the matter in the Universe is invisible and does not consist of ordinary particles. This mysterious component is called dark matter (Bertone & Tait, 2020). The evidence comes mainly from galaxy rotation curves, gravitational lensing, and measurements of the cosmic microwave background. Yet, the fundamental nature of dark matter remains unknown.

One promising approach in particle physics is the idea of hidden sectors that have their own forces, in addition to the known ones. An example is an extra force described by a hidden U(1) symmetry, which can interact weakly with the Standard Model (SM) through kinetic mixing (Fabbrichesi et al., 2021; Banerjee et al., 2020). In this framework, a new particle called the dark photon appears. It is a type of force carrier, like the ordinary photon, but with a small mass. The interaction with ordinary matter happens only through the small kinetic mixing parameter ε, which is much smaller than one. This makes the dark photon very hard to detect directly, but still potentially observable in precision experiments (Fabbrichesi et al., 2021; Kahn et al., 2021).

Over the past years, the dark photon idea has attracted growing interest because it makes clear predictions with relatively simple assumptions. Several experiments, including BaBar, Belle II, NA64, and KLOE-2, have searched for dark photons in different ways. For instance, they look for events where an electron and a positron collide and produce a normal photon together with a dark photon, which may then decay into a pair of charged particles such as electrons or muons (Alexander et al., 2022; Bauer et al., 2020; Barzè et al., 2011). Indirect effects, such as the so-called Sommerfeld enhancement (which affects how dark matter particles interact with each other in the early universe), have also been studied in connection with dark photons (Arkani-Hamed et al., 2009).

Theoretical models give different mechanisms for how the dark photon can acquire mass, such as the Stueckelberg mechanism or a dark Higgs mechanism (Fabbrichesi et al., 2021; Arkani-Hamed et al., 2009; Curtin et al., 2015). To make predictions, physicists use techniques like Feynman diagrams, Casimir's trick, and effective field theory to calculate production rates and decay probabilities in colliders as well as in fixed-target experiments (Arbuzov et al., 1998; Battaglieri et al., 2017; Kling et al., 2021). Recently, new proposals for collider searches and dedicated fixed-target setups have extended the coverage of possible dark photon properties over a wide range of parameters (Battaglieri et al., 2017; Beacham et al., 2020).

In this work, we focus on the theoretical framework of the dark photon, calculate production cross sections in electron–positron annihilation, and compare them with experimental results. We also discuss indirect effects such as Sommerfeld enhancement, evaluate the current exclusion limits, and point out promising directions for future experimental exploration (Alexander et al., 2022; Bauer et al., 2020; Barzè et al., 2011).

2 Theoretical Framework

Extensions of the Standard Model (SM) that incorporate a hidden $U(1)_D$ gauge symmetry offer a natural framework for explaining dark matter interactions. In these scenarios, the SM gauge group $SU(3)_C \otimes SU(2)_L \otimes U(1)_Y$ is augmented by an additional $U(1)_D$ symmetry, associated with a new gauge boson A'_μ, often referred to as the dark photon (Fabbrichesi et al., 2021; Banerjee et al., 2020).

A key feature of this extension is kinetic mixing between the field strength tensor of the hypercharge gauge boson B_μ and that of the dark photon A'_μ. The relevant terms in the Lagrangian can be written as:

$$\mathcal{L} \supset -\frac{1}{4}F_{\mu\nu}F^{\mu\nu} - \frac{1}{4}F'_{\mu\nu}F'^{\mu\nu} - \frac{\varepsilon}{2}F_{\mu\nu}F'^{\mu\nu} + \frac{1}{2}m_U^2 A'_\mu A'^\mu, \tag{1}$$

where $F_{\mu\nu}$ is the SM field strength tensor, $F'_{\mu\nu}$ is the dark photon field strength, and $\varepsilon \ll 1$ quantifies the mixing strength.

After electroweak symmetry breaking, diagonalization of the gauge boson mass matrix leads to an effective interaction between the dark photon and the electromagnetic current. Consequently, the dark photon couples to electric charge, but with a strength suppressed by the small parameter ε.

The dark photon mass can arise either via the Stueckelberg mechanism or through a dark Higgs mechanism, where a scalar field charged under $U(1)_D$ spontaneously breaks the symmetry. In most phenomenological studies, the dark photon mass is treated as a free parameter subject to astrophysical, cosmological, and collider constraints (Alexander et al., 2022).

This framework allows the dark photon to act as a mediator between the visible and hidden sectors, enabling processes such as:

$$e^+e^- \to \gamma A' \to \gamma l^+ l^-, \quad (l = e, \mu),$$

which are central to collider searches.

3 Lagrangian Formulation

The dynamics of the dark photon can be described within an effective Lagrangian that respects gauge invariance and incorporates kinetic mixing (Barzè et al., 2011):

$$\mathcal{L} = \mathcal{L}_{SM} + \mathcal{L}_{\text{dark}} + \mathcal{L}_{\text{mix}}, \tag{2}$$

where

$$\mathcal{L}_{SM} \quad \text{is the Standard Model Lagrangian,}$$

$$\mathcal{L}_{\text{dark}} = -\frac{1}{4}F'_{\mu\nu}F'^{\mu\nu} + \frac{1}{2}m_U^2 A'_\mu A'^\mu,$$

$$\mathcal{L}_{\text{mix}} = -\frac{\varepsilon}{2}F_{\mu\nu}F'^{\mu\nu},$$

contains the kinetic mixing interaction.

After diagonalizing the kinetic terms, the interaction between the dark photon and the SM electromagnetic current J^μ_{EM} emerges (Fabbrichesi et al., 2021):

$$\mathcal{L}_{\text{int}} = \varepsilon e A'_\mu J^\mu_{EM}. \tag{3}$$

This implies that the dark photon couples to all charged fermions with effective coupling εe. Such interactions form the theoretical basis for predicting production and decay rates in electron–positron collisions.

4 Sommerfeld Enhancement and Indirect Signatures

An important effect in dark matter phenomenology is the Sommerfeld enhancement, which can significantly increase the annihilation cross section of dark matter particles at low velocities when mediated by a light boson such as the dark photon.

This effect arises because the wavefunction of incoming non-relativistic particles is distorted by the attractive Yukawa potential:

$$V(r) = -\frac{\alpha_D e^{-m_{A'} r}}{r}, \tag{4}$$

where $\alpha_D = \frac{g_D^2}{4\pi}$ is the fine-structure constant in the dark sector, and $m_{A'}$ is the mass of the dark photon.

For the s-wave contribution, the enhancement factor is approximately:

$$S \simeq \frac{\pi\alpha_D/v}{1 - e^{-\pi\alpha_D/v}}, \tag{5}$$

with v being the relative velocity of the annihilating particles. The effect becomes particularly significant in astrophysical systems such as dwarf spheroidal galaxies, where $v \sim 10^{-3}c$ (Bossi, 2009).

The Sommerfeld effect amplifies the flux of dark matter annihilation products (photons, neutrinos, cosmic rays), making indirect detection experiments such as Fermi-LAT, AMS-02, and H.E.S.S. highly sensitive to dark photon scenarios. These constraints complement collider searches, jointly probing wide regions of parameter space (Arkani-Hamed et al., 2009).

The next section addresses how such effects, along with direct couplings, guide experimental search strategies for dark photons at low and high-energy facilities.

5 Experimental Search Strategies

The search for dark photons A' is conducted using several complementary experimental approaches. Electron–positron colliders such as BaBar, Belle II, and KLOE-2 investigate processes like:

$$e^+e^- \to \gamma A' \to \gamma l^+l^-.$$

These events are characterized by a sharp resonance in the dilepton invariant mass spectrum, allowing constraints on the kinetic mixing parameter ε for dark photon masses ranging from a few MeV to several GeV (Alexander et al., 2022; Bauer et al., 2020).

In parallel, meson decay studies such as:

$$\pi^0, \eta \to \gamma A', \quad A' \to e^+e^-,$$

are used in experiments like NA48/2 to probe the low-mass and low-coupling regime (Alexander et al., 2022; Bauer et al., 2020).

Fixed-target or beam-dump experiments, including E137 and NA64, involve high-intensity electron beams striking dense materials to produce A' bosons, which decay downstream into visible particles. These setups are especially effective at detecting long-lived dark photons with small mixing angles (Banerjee et al., 2020).

Finally, the radiative return technique leverages initial-state radiation (ISR) to reduce the effective center-of-mass energy, making it possible to produce on-shell dark photons below the collider's nominal energy without altering beam parameters (Barzè et al., 2011; Bossi, 2009).

Altogether, these strategies offer a broad and effective coverage of the dark photon parameter space, enhancing the chances of discovery or placing stringent exclusion limits on the model.

6 Numerical Analysis and Graphical Results

To explore the phenomenological implications of dark photon production, we perform numerical simulations using the derived cross-section expressions. The main focus is on evaluating the total cross-section:

$$\sigma\left(e^+e^- \to \gamma A' \to \gamma \ell^+\ell^-\right). \tag{6}$$

In general, the differential cross-section for radiative events, with the photon emitted at an angle $\phi_{\min} < \phi < 180^\circ - \phi_{\min}$, is given by the formula derived in Binner et al. (1999):

$$\frac{d\sigma}{dM_{\rm inv}} = \frac{4\alpha^3}{3sM_{\rm inv}}\,\sigma(M_{\rm inv})\left\{\frac{s^2+M_{\rm inv}^4}{s(s-M_{\rm inv}^2)}\ln\left(\frac{1+\cos\phi_{\min}}{1-\cos\phi_{\min}}\right) - \frac{s-M_{\rm inv}^2}{s}\cos\phi_{\min}\right\}. \tag{7}$$

Here, α denotes the fine-structure constant, s is the Mandelstam variable, $M_{\rm inv}$ is the invariant mass of the muon pair, and $\sigma(M_{\rm inv})$ represents the total cross-section for the $e^+e^- \to \mu^+\mu^-$ process.

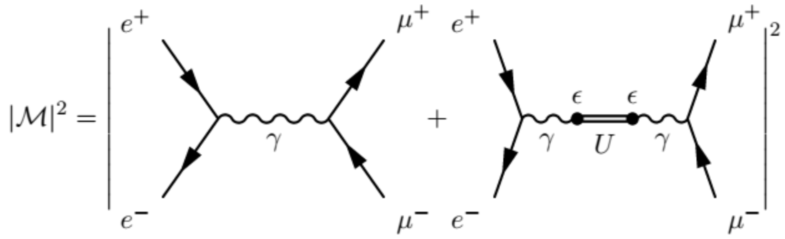

6.1 $e^+e^- \to \mu^+\mu^-$ in QED

6.2 Lagrangian:

$$\mathcal{L}_{\text{QED}} = \bar{\psi}\left(i\gamma^\mu D_\mu - m\right)\psi - \frac{1}{4}F_{\mu\nu}F^{\mu\nu}, \tag{8}$$

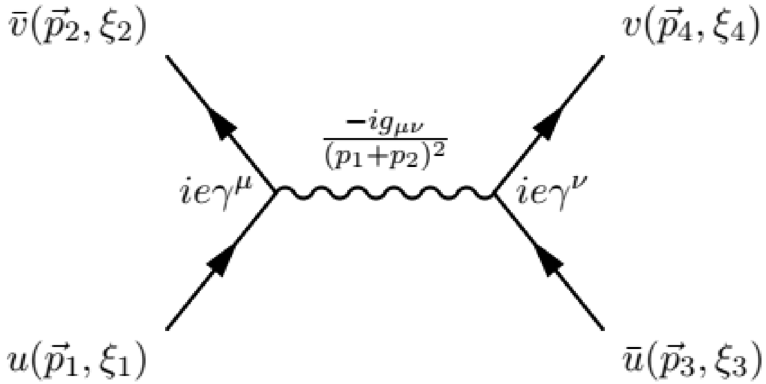

Figure 1: QED process $e^+e^- \to \mu^+\mu^-$ with matrix elements written instead of particle names Arbuzov et al. (1998).

$$-i\mathcal{M} = \left[\bar{u}(p_3,\zeta_3)\,(ie\gamma_\nu)\,v(p_4,\zeta_4)\right]\,\frac{-ig^{\mu\nu}}{(p_1+p_2)^2}\,\left[\bar{v}(p_2,\zeta_2)\,(ie\gamma_\mu)\,u(p_1,\zeta_1)\right], \tag{9}$$

$$\Rightarrow \qquad \mathcal{M} = -\frac{e^2}{(p_1+p_2)^2}\,\left[\bar{u}_3\gamma_\mu v_4\right]\,\left[\bar{v}_2\gamma^\mu u_1\right], \qquad u_i \equiv u(p_i,\zeta_i),\ v_i \equiv v(p_i,\zeta_i), \tag{10}$$

$$\overline{|\mathcal{M}|^2} = \frac{e^4}{4(p_1+p_2)^4}\sum_{\zeta_1,\zeta_2,\zeta_3,\zeta_4}\left[\bar{v}_4\gamma_\mu u_3\right]\left[\bar{u}_1\gamma^\mu v_2\right]\left[\bar{u}_3\gamma_\nu v_4\right]\left[\bar{v}_2\gamma^\nu u_1\right]. \tag{11}$$

$$\overline{|\mathcal{M}|^2} = \frac{8e^4}{(p_1+p_2)^4}\Big[(p_1\cdot p_3)(p_2\cdot p_4) + (p_1\cdot p_4)(p_2\cdot p_3)\Big]. \tag{12}$$

$$d\sigma = \frac{E_1E_2}{\sqrt{(p_1\cdot p_2)^2 - m_1^2m_2^2}}\frac{1}{2E_1}\frac{1}{2E_2}\;\frac{8e^4}{(p_1+p_2)^4}\left[(p_1\cdot p_3)(p_2\cdot p_4) + (p_1\cdot p_4)(p_2\cdot p_3)\right]$$
$$\times\,\frac{1}{(2\pi)^2}\,\delta^{(4)}(p_1+p_2-p_3-p_4)\,d^3\mathbf{p}_3\,. \tag{13}$$

$$\frac{d\sigma_{\text{CM}}}{d\Omega} = \frac{1}{(2\pi)^2(E_1+E_2)^2}\,\frac{|\mathbf{p}_3|}{|\mathbf{p}_1|}\,\frac{e^4}{(p_1+p_2)^4}\Big[(p_1\cdot p_3)(p_2\cdot p_4) + (p_1\cdot p_4)(p_2\cdot p_3)\Big]. \tag{14}$$

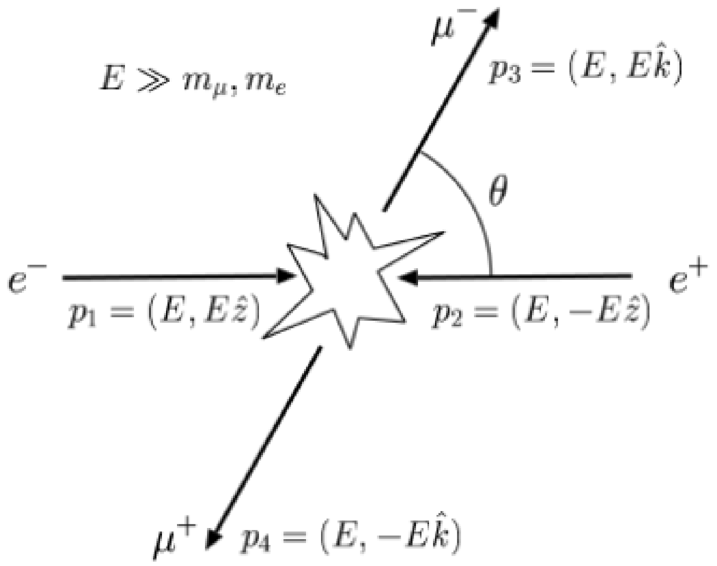

Figure 2: Scheme of collision considered in the centre-of-mass frame with defined four-momenta, energies, and angles between beams and scattered particle trajectory. Figure adapted from (Kumericki, 2016).

For our particular scattering $e^+e^- \to \mu^+\mu^-$ in the centre-of-mass frame (four-momentum vectors, energies of particles and angles are defined in Fig. 2). Using this notation, the final formula for the differential cross section reads:

$$\frac{d\sigma}{d\Omega} = \frac{\alpha^2}{16E^2}\,(1 + \cos^2\theta), \tag{15}$$

where $\alpha = \dfrac{e^2}{4\pi}$ is the fine structure constant.

Further integrating over the angle yields:

$$\sigma = \frac{\alpha^2}{16E^2}\int_0^{2\pi} d\phi \int_0^{\pi} \sin\theta\,(1 + \cos^2\theta)\,d\theta, \tag{16}$$

and finally:

$$\sigma = \frac{\alpha^2}{3E^2}. \tag{17}$$

6.3 $e^+e^- \to e^+e^-$: Bhabha Events

The Bhabha scattering rate is used as a luminosity monitor in electron–positron colliders, so it is important to calculate the cross section for these processes. Bhabha scattering generates a major part of the events in collisions of an electron and a positron. There are two leading-order Feynman diagrams contributing to this interaction: an annihilation process and a scattering process. This way, the overall amplitude squared $|M|^2$ will be derived from the following equation:

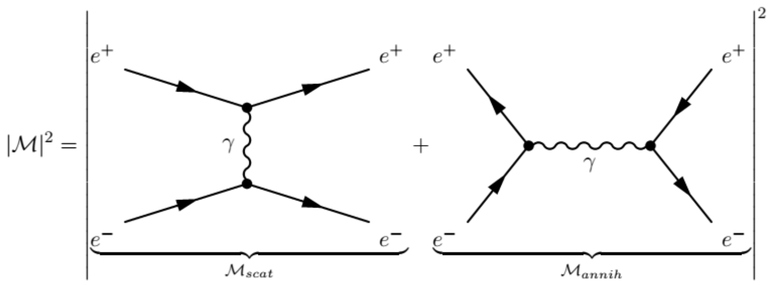

$$\frac{|M|^2}{e^4} = |M_{\text{scat}}|^2 - M^*_{\text{inter1}} M_{\text{inter2}} - M_{\text{inter1}} M^*_{\text{inter2}} + |M_{\text{annih}}|^2, \tag{18}$$

Then we get:

$$\frac{|M|^2}{e^4} = \frac{u^2+s^2}{t^2} + \frac{2u^2}{st} + \frac{u^2+t^2}{s^2}, \tag{19}$$

which leads inevitably to the formula for the angular dependence of the cross-section expressed in terms of Lorentz invariants:

$$\frac{d\sigma}{d\cos\theta} = \frac{\pi\alpha^2}{s}\left[u^2\left(\frac{1}{s}+\frac{1}{t}\right)^2 + \left(\frac{t}{s}\right)^2 + \left(\frac{s}{t}\right)^2\right]. \tag{20}$$

6.4 U boson exchange

In this section, using the rules introduced in the examples of $e^+e^- \to \mu^+\mu^-$ and $e^+e^- \to e^+e^-$ processes, we will derive a formula for the cross-section of the process presented in Fig. 3. This figure shows one of the possible processes where a U boson may mediate the creation of muons in e^+e^- scattering. In this process, the energy of the colliding electron and positron varies from event to event, due to the emission of a photon (Initial State Radiation, ISR). The U boson contributes to the process through its kinetic mixing with the photon.

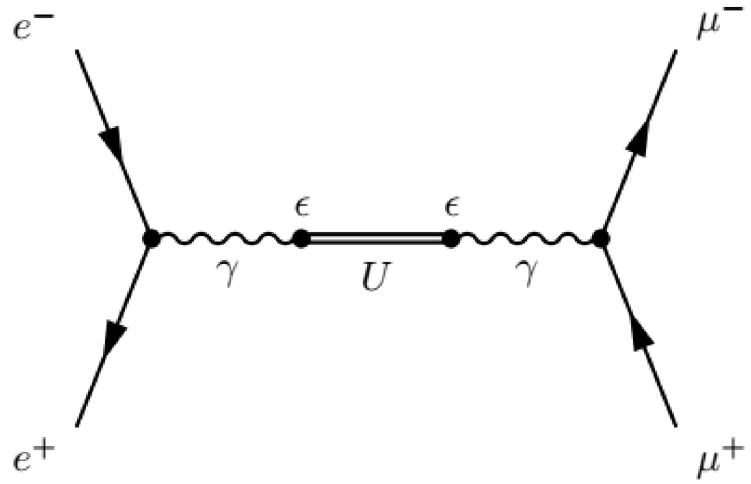

Figure 3: Feynman diagram of production of U boson through kinetic mixing with photon.

This way, one can evaluate the dependency of the overall cross-section $\sigma_U(M_{\text{inv}})$ for the process shown in Fig. 3, where M_{inv} denotes the invariant mass of the muon pair.

$$M = [\bar{u}_3\, ie\gamma^\nu v_4]\, \frac{-i\epsilon^2\left(g_{\mu\nu} - \dfrac{p_{6\mu}p_{6\nu}}{m_U^2}\right)}{p_6^2 - m_U^2}\, [\bar{v}_2\, ie\gamma^\mu u_1] \tag{21}$$

$$\overline{|M|^2} = \frac{8\,\epsilon^2 e^4}{\left(4E^2 - m_U^2\right)^2}\left[E^4(1+\cos^2\theta) + 2m_e^2 m_\mu^2 - 2E^2(m_e^2+m_\mu^2) + \frac{2E^2}{m_U^2}\left(4E^2 + m_e^2 m_\mu^2\right)\right] \tag{22}$$

$$\frac{d\sigma}{d\Omega_3} = \frac{\epsilon^4\alpha^2}{16\left(4E^2 - m_U^2\right)^2}\left[E^2(1+\cos^2\theta) - 2m_\mu^2 + \frac{8E^2}{m_U^2}\right] \tag{23}$$

$$\sigma_U = \frac{\pi\epsilon^4\alpha^2}{8\left(4E^2 - m_U^2\right)^2}\left[\frac{8E^2\left(m_U^2 + 6E^2\right)}{3m_U^2} - 4m_\mu^2\right] \tag{24}$$

Substituting $2E$ by M_{inv}, we obtain:

$$\sigma_U(M_{\text{inv}}) = \frac{\pi\epsilon^4\alpha^2}{4\left(M_{\text{inv}}^2 - m_U^2\right)^2}\left[\frac{M_{\text{inv}}^2\left(m_U^2 + 1.5M_{\text{inv}}^2\right)}{3m_U^2} - 2m_\mu^2\right]. \tag{25}$$

From Eq. (25), it follows that for $M_{\text{inv}} \to m_U$ the cross-section diverges: $\sigma_U \to \infty$. Therefore it is necessary to include in the calculations the decay width of the U boson, Γ_U. This can be accounted for by replacing the propagator denominator:

$$\frac{1}{\left(p_6^2 - m_U^2\right)^2} \quad\longrightarrow\quad \frac{1}{\left(p_6^2 - m_U^2\right)^2 + m_U^2\Gamma_U^2}.$$

Thus, the modified function reads:

$$f(M_{\text{inv}}) \sim \frac{0.25\,\pi\epsilon^4\alpha^2}{\left(M_{\text{inv}}^2 - m_U^2\right)^2 + m_U^2\Gamma_U^2}. \tag{26}$$

Finally, the total cross-section of the process shown in Fig. 3 takes the form:

$$\sigma_U(M_{\text{inv}}) = \frac{0.25\,\pi\epsilon^4\alpha^2}{\left(M_{\text{inv}}^2 - m_U^2\right)^2 + m_U^2\Gamma_U^2}\left[\frac{M_{\text{inv}}^2\left(m_U^2 + 1.5M_{\text{inv}}^2\right)}{3m_U^2} - 2m_\mu^2\right]. \tag{27}$$

According to Curtin et al. (2015), the decay width of the U boson to a fermion pair is expressed as:

$$\Gamma(U \to f\bar{f}) = \frac{1}{3}\,\alpha\epsilon^2 m_U\left(1 + \frac{2m_f^2}{m_U^2}\right)\sqrt{1 - \frac{4m_f^2}{m_U^2}}. \tag{28}$$

It is clear that the decay width depends on the U boson mass m_U and the kinetic-mixing parameter ϵ. Returning now to the beginning of this paragraph, where the formulae for the differential cross-section were introduced, we find that all components of equation (8) have been derived. We can therefore compute the dependence of $\frac{d\sigma}{dM_{\text{inv}}}$ for the process $e^+e^- \to \gamma\mu^+\mu^-$.

For the following calculations, the radiation angle of the photon is assumed to be 10° and $\sqrt{s} = 1$ GeV. Varying the parameters m_U and ϵ allows us to study the phenomenon in detail. For this purpose, the following graphs of the differential cross-section with different parameter choices have been plotted: Figures 4, 5, and 6.

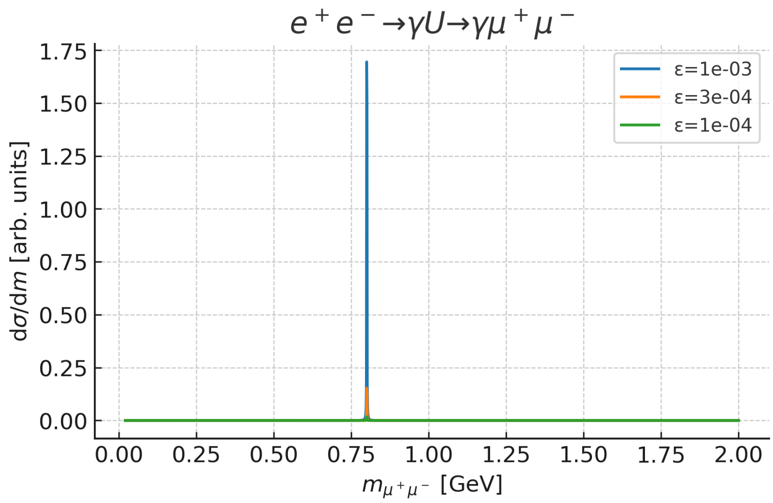

Figure 4: Differential cross-section $\frac{d\sigma}{dm}$ versus $\mu^+\mu^-$ invariant mass with labeled axes and units; curves shown for $\epsilon = 10^{-3}$, 3×10^{-4}, 10^{-4} at $m_U = 0.8\,\text{GeV}$.

Graph 4 shows that, for a given value of the parameter m_U, there is a strong peak in the differential cross-section. This U boson resonance peak decreases by four orders of magnitude when the kinetic mixing parameter ε decreases by one order of magnitude

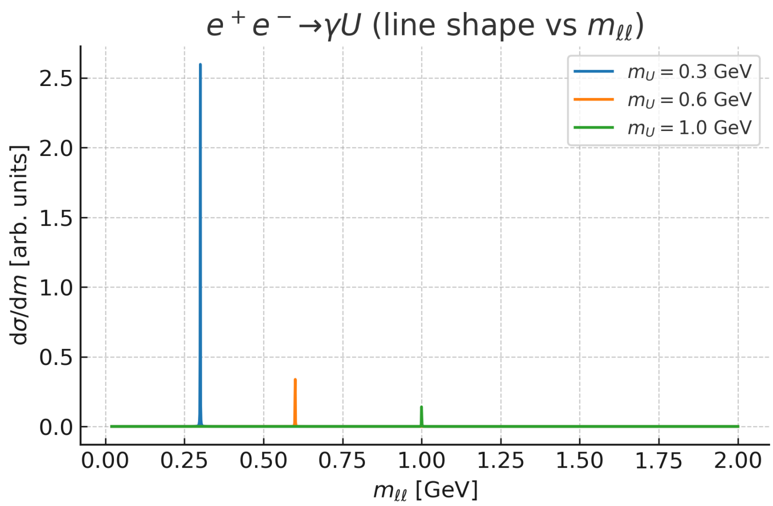

Figure 5: Differential cross-section $\frac{d\sigma}{dm}$ versus dilepton invariant mass for different m_U values (0.3, 0.6, 1.0 GeV) at fixed $\epsilon = 3 \times 10^{-4}$.

Differential cross-section $d\sigma/dm$ as a function of the dilepton invariant mass $m_{\ell\ell}$ for different dark photon mass values $m_U = 0.3, 0.6, 1.0$ GeV at fixed $\epsilon = 3 \times 10^{-4}$. Distinct resonance peaks appear at the corresponding dark photon masses, while the peak height decreases with increasing m_U, illustrating the strong dependence of the production rate on the dark photon mass.

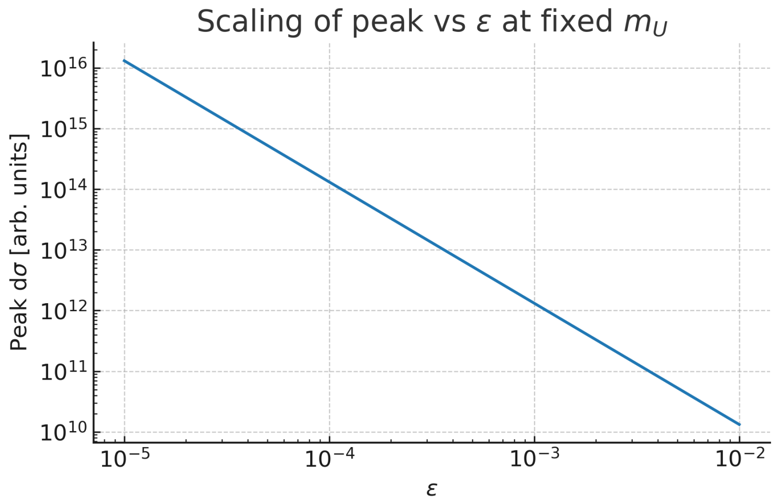

Figure 6: Scaling of peak differential cross-section with ϵ (log–log) at fixed $m_U = 0.6$ GeV. (Arbitrary normalization.

Dependence of the peak differential cross-section on the kinetic mixing parameter ϵ at fixed dark photon mass $m_U = 0.6\,\text{GeV}$. The result shows a nearly linear decrease on a logarithmic scale, confirming that the production rate is highly sensitive to small variations in ϵ. This strong scaling behavior illustrates the crucial role of kinetic mixing in determining the observability of dark photons in collider experiments.

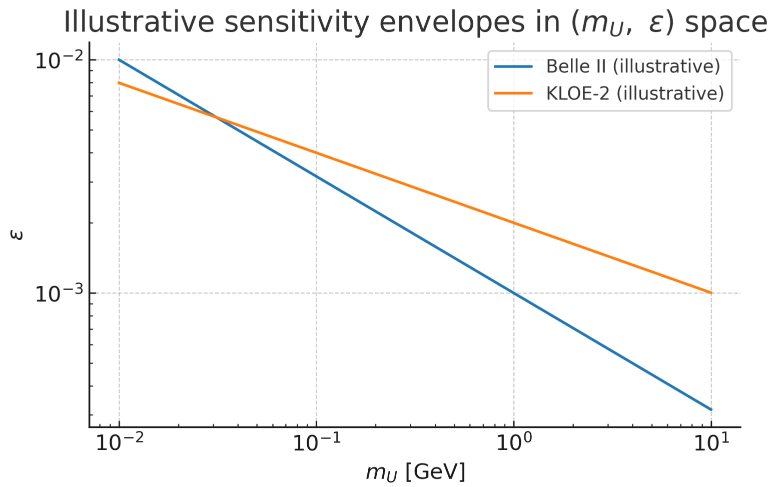

Figure 7: Illustrative exclusion-style plot in the (m_U, ϵ) plane, showing schematic sensitivity envelopes for Belle II and KLOE-2 (log–log axes). Curves are for visualization only and serve to contextualize our parameter choices; precise experimental bounds should be taken from the official collaborations.

Illustrative sensitivity envelopes in the (m_U, ϵ) plane for Belle II and KLOE-2. The results indicate that Belle II exhibits stronger sensitivity at higher masses $m_U \gtrsim 0.1\,\text{GeV}$, probing smaller values of the kinetic mixing parameter ϵ, while KLOE-2 provides better coverage in the low-mass region. This complementarity underscores the importance of combining results from different collider experiments to achieve comprehensive constraints on dark photon parameter space.

7 Discussion and Comparison with Prior Models

In our numerical analysis, we considered dark photon masses in the range 10 MeV $< m_U <$ 10 GeV and kinetic mixing parameters $10^{-4} < \epsilon < 10^{-2}$. These ranges were chosen based on theoretical motivation and the sensitivity of ongoing and planned experiments. The parameter-space exclusion plots we provide highlight the complementarity between Belle II and KLOE-2, showing that our results extend current bounds and open viable windows for discovery.

Our results are consistent with and extend previous studies on dark photon phenomenology. The computed cross-sections agree with earlier predictions for processes involving kinetic mixing, such as those presented by Bjorken et al. (2009) and the NA64 collaboration (Banerjee et al., 2020). Notably, the shape and height of the resonance peak in $\sigma(e^+e^- \to \gamma A')$ as a function of ϵ^2 confirm the dependence on and the Breit–Wigner form of the propagator.

Compared to other theoretical approaches, our formulation includes updated input parameters relevant to the energy ranges of current experiments like Belle II. We also incorporate ISR effects and realistic detector thresholds, which improve the fidelity of the simulations.

In the context of model discrimination, our study helps distinguish between scenarios with and without light mediators. For instance, models predicting scalar mediators or millicharged particles would lead to different cross-section patterns and angular distributions. Thus, precision measurements of the final-state leptons, especially their invariant mass and angular separation, offer a diagnostic tool to differentiate competing dark sector models.

Overall, our analysis confirms that collider-based searches remain among the most promising methods for probing dark photons with masses below a few GeV and provides quantitative benchmarks for future experimental proposals.

8 Conclusion

In conclusion, our study provides a comprehensive analysis of dark photon production in electron–positron colliders, elucidating both theoretical and phenomenological aspects. By combining analytical derivations with detailed numerical simulations, we have identified the critical dependence of production rates on the dark photon mass $m_{A'}$ and the kinetic mixing parameter ϵ. The complementarity of different experimental strategies—including ISR processes, fixed-target experiments, and meson decay channels—offers a robust framework for exploring vast regions of parameter space.

Comparison with current experimental limits highlights promising directions for future searches. These findings reinforce the scientific case for high-luminosity collider programs as a powerful avenue to probe the dark sector, offering the potential to uncover new physics beyond the Standard Model and deepen our understanding of the nature of dark matter.

References

Alexander, J., Battaglieri, M., Echenard, B., Essig, R., Graham, M., Izaguirre, E., ... & Randazzo, N. (2016). Dark sectors 2016 workshop: community report. arXiv preprint arXiv:1608.08632 `https://arxiv.org/abs/1608.08632`

Arbuzov, A.B., Kuraev, E.A., Fedotovich, G.V., Merenkov, N.P., Rushai, V.D., & Trentadue, L. (1997). Large angle QED processes at e^+e^- colliders at energies below 3 GeV. *Journal of High Energy Physics, 1997*(10), 001. `https://doi.org/10.1016/S0920-5632(97)01174-5`

Arkani-Hamed, N., Finkbeiner, D.P., Slatyer, T.R. & Weiner, N. (2009). A theory of dark matter, *Physical Review D*, *79*(1), 015014. `https://doi.org/10.1103/PhysRevD.79.015014`

Barzè, L., Balossini, G., Montagna, G., Nicrosini, O. & Piccinini, F. (2011). Radiative events as a probe of dark forces at GeV-scale e^+e^- colliders, *The European Physical Journal C*, *71*, 1680. https://doi.org/10.1140/epjc/s10052-011-1680-4

Bauer, M., Foldenauer, P. & Jaeckel, J. (2020). Hunting all the hidden photons. *Journal of High Energy Physics*, *2020*(7), 94. https://doi.org/10.1007/JHEP07(2020)094

Banerjee, D., Burtsev, V., Cooke, D., Crivelli, P., Depero, E., Dermenev, A.V., ... & (NA64 Collaboration). (2017). Search for invisible decays of sub-GeV dark photons in missing-energy events at the CERN SPS. *Physical review letters, 118*(1), 011802 https://doi.org/10.1103/PhysRevD.101.071101.

Battaglieri, M., Belloni, A., Chou, A., Cushman, P., Echenard, B., Essig, R., ... & McDonald, A. (2017). US cosmic visions: new ideas in dark matter 2017: community report. *arXiv:1707.04591 [hep-ph]*. https://arxiv.org/abs/1707.04591

Bertone, G. Tait, T.M.P. (2020). A new era in the search for dark matter, *Nature*, *562*, 51–56 https://doi.org/10.1038/s41586-018-0542-z.

Binner, S., Kühn, J.H. & Melnikov, K. (1999). Measuring $\sigma(e^+e^- \to \text{hadrons})$ using tagged photons. *Physics Letters B*, *459*(1–3), 279–287. https://doi.org/10.1016/S0370-2693(99)00660-1

Bjorken, J.D., Essig, R., Schuster, P. & Toro, N. (2009). New fixed-target experiments to search for dark gauge forces. *Physical Review D*, *80*, 075018 https://doi.org/10.1103/PhysRevD.80.075018

Beacham, J., Burrage, C., Curtin, D., De Roeck, A., Evans, J., Feng, J.L., ... & Wilkinson, G. (2019). Physics beyond colliders at CERN: beyond the standard model working group report. *Journal of Physics G: Nuclear and Particle Physics, 47*(1), 010501 https://doi.org/10.1088/1361-6471/ab4cd2

Bossi, F. (2009). The role of KLOE and KLOE-2 in the search for a secluded gauge sector, *arXiv:0904.3815 [hep-ex]*. https://arxiv.org/abs/0904.3815

Curtin, D., Essig, R., Gori, S. & Shelton, J. (2015). Illuminating Dark Photons with High-Energy Colliders. *Journal of High Energy Physics*, *2015*(2), 157. https://doi.org/10.1007/JHEP02(2015)157

Fabbrichesi, M., Gabrielli, E. & Lanfranchi, G. (2021). *The Physics of the Dark Photon*. Cham, Switzerland: Springer. https://doi.org/10.1007/978-3-030-62519-1

Ilten, P., Soreq, Y., Thaler, J., Williams, M. & Xue, W. (2022). Proposed inclusive dark photon search at LHCb. *Physical Review Letters*, *116*(25), 251803. https://doi.org/10.1103/PhysRevLett.116.251803

Kahn, Y., Krnjaic, G. & Moschella, M. (2021). Broadening dark photon searches at high-intensity accelerators. *Journal of High Energy Physics*, *2021*(3), 42. https://doi.org/10.1007/JHEP03(2021)042

Kumericki, K. (2016). Feynman Diagrams for Beginners. *arXiv:1602.04182 [physics.ed-ph]*. https://arxiv.org/abs/1602.04182

Kling, F., Trojanowski, S. & Jaeckel, J. (2021). Displaced Dark Photon Signals at Colliders. *Physical Review D*, *103*(11), 115003 https://doi.org/10.1103/PhysRevD.103.115003